Fiber Optic Electric Field Intensity Sensor Based on Liquid Crystal-Filled Photonic Crystal Fiber Incorporated Ring Laser

Yibin Liu, Weihao Lin, Mang I Vai, *Senior Member, IEEE*, Perry Ping Shum, *Senior Member, IEEE*, Li-Yang Shao, *Senior Member, IEEE*, Wei He, Shuaiqi Liu, Fang Zhao, Weizhi Wang, and Yuhui Liu

***Abstract*—Optical fiber sensors are of splendid strength for electrical field intensity sensor due to characteristics including the immunity to electromagnetic interference, lightweight, high sensitivity, and large bandwidth. In this paper, we proposed an electric field intensity sensor based on Mach-Zehnder interferometer (MZI) based liquid crystal (LC) filled photonic crystal fiber (PCF) embedded in optical fiber ring laser (FRL). The air hole of PCF combines the LC and fiber core together. When LC is introduced into air holes, it can maintain the waveguide based on external parameters. The photonic bandgap effect significantly improved the sensitivity between light and external electrical field intensity. Thanks to the FRL demodulation, a high signal to noise ratio (SNR) spectrum about 35 dB is obtained. Besides, in comparison with traditional LC-PCF structures, the sensitivity of ours is as high as 1.1 nm/Vrms which is about twice than traditional sensors. At the same time, the stability of proposed sensor was verified which fluctuation was 0.15 nm around 2.5 hours. Therefore, our structure is expected to practical applications in remote electric field monitor and such electric modulate electro-optical devices.**

***Index Terms*—Fiber ring laser, liquid crystal, photonic crystal fiber.**

Manuscript received October 8, 2021; revised December 1, 2021; accepted December 16, 2021. Date of publication December 21, 2021; date of current version January 13, 2022. This work was supported in part by the startup fund from Southern University of Science and Technology, Shenzhen government and Future Greater-Bay Area Network Facilities for Large-scale Experiments and Applications under Grant LZC0019, in part by The Verification Platform of Multi-tier Coverage Communication Network for Oceans under Grant LZC0020, in part by the Guangdong Department of Science and Technology under Grant 2021A0505080002, in part by Shenzhen Science, Technology and Innovation Commission under Grant 20200925162216001, and in part by the Guangdong Department of Education under Grant 2021ZDZX1023. *(Yibin Liu and Weihao Lin contributed equally to this work.) (Corresponding author: Li-Yang Shao.)*

Yibin Liu, Perry Ping Shum, Wei He, Fang Zhao, and Yuhui Liu are with the Department of Electrical and Electronic Engineering, Southern University of Science and Technology, Shenzhen 518055, China (e-mail: 11811808@mail.sustech.edu.cn; shenp@sustech.edu.cn; 11813105@mail.sustech.edu.cn; 12031197@mail.sustech.edu.cn; 12068026@mail.sustech.edu.cn).

Weihao Lin and Shuaiqi Liu are with the Department of Electrical and Electronic Engineering, Southern University of Science and Technology, Shenzhen 518055, China, and also with the State Key Laboratory of Analog and Mixed-Signal VLSI, University of Macau, Macau 999078, China (e-mail: 11510630@mail.sustech.edu.cn; 11853004@mail.sustech.edu.cn).

Mang I Vai is with the State Key Laboratory of Analog and Mixed-Signal VLSI, University of Macau, Macau 999078, China (e-mail: fstmiv@um.edu.mo).

Li-Yang Shao is with the Department of Electrical and Electronic Engineering, Southern University of Science and Technology, Shenzhen 518055, China, and also with the Peng Cheng Laboratory, Shenzhen 518005, China (e-mail: shaoly@sustech.edu.cn).

Weizhi Wang is with the Peng Cheng Laboratory, Shenzhen 518005, China (e-mail: wangwzh@pcl.ac.cn).

Digital Object Identifier 10.1109/JPHOT.2021.3136879

I. Introduction

In THE past few years, optical fiber electric-field sensors have significantly potential requirement in intensive distributed electromagnetic field. The intensive power machine attached with distributed electromagnetic field make it impossible to measure electric and electronic field at work state [1]. Due to small volume, great portability, high sensitivity, and immunity to electro-magnetic interference [2], varieties optical fiber electric-field sensors have been investigated and studied to measure electric field intensity in the laboratory, such as tilted fiber grating (FBG) [3], hole-core fiber (HCF) [4], side-hole fiber (SHF) [5], FBG [6] and bandgap like effect [7]. All the optical fiber sensor information is carried in the light that has no destructions on electromagnetic field.

LC, as a typical optoelectronic modulation material, has been widely used in various optoelectronic device. The optical parameter of LC such as reflective index and refractive index can be easily controlled by external electric field. The low relaxation time of LC and higher refractive index (RI) than silicon make it suitable for optical fiber device. Recently, the PCF combined with LC is proposed and all work to date has focused on tuning the PCF band-gap effect completely or partially filled LC [8], [9]. The PCF can be modulated by LC since its pores can be easily filled in capillary effect. Because the RI of LC is much higher than silicon glass, the total internal reflection of PCF turns out to be photonic bandgap (PBG) effect. L Wei *et al.* demonstrated the LC-filled PCF and worked as an electrooptic modulator with a sensitivity of 0.42 nm/V [10]. Du *et al.* successfully realized electric field measurement by using photonic band-gap fiber to form Sagnac ring for liquid crystal filling, with a sensitivity of 0.53 nm/V [11]. However, LC full leads to high trans-mission loss, burrs and lower accuracy. Recently, Huang *et al.* used liquid crystals to accurately fill the air holes in the inner layer of PCF to form a fiber electric field modulation coupler with a sensitivity of 5.594 nm/V [12]. However, although the LC-filled PCF shows an incredible improvement in electric field sensing, the demodulator based on broadband light sources limit its application on the laboratory.

For the research content of some specific applications of electric field sensing, Lao *et al.* used tilted fiber grating to

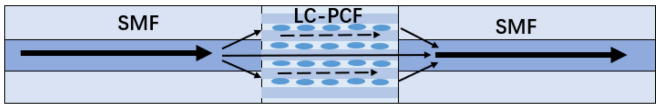

Fig. 1. Schematic of the designed LC-PCF.

comprehensively monitor the electrochemical activity of supercapacitors [13]. P. Sezemsky *et al.* devoted themselves to studying the recognition characteristics of indium tin oxide (ITO) films by using electrical field sensors [14]. Jiaqiang Huang *et al.* used an electrochemical workstation to simultaneously measure temperature and refractive index changes inside the battery, which are related to chemical changes of electrolyte [15]. These specific application scenarios prove that electric field sensors have broad application space.

In this paper, we propose a MZI based on LC filled PCF as electric field intensity modulation sensor in a FRL. The interference between the cladding mode filled with LC and the core mode result in the interference resonance wavelength in the transmission spectrum. In the experiment, the resonant wavelength range is from 1530 nm to 1575 nm in the near infrared band with an average sensitivity of 1.11 nm/Vrms. Because of the FRL, the signal to noise ratio of output spectrum is up to 35 dB, and the 3-dB bandwidth is less than 0.15 nm. At the same time, the stability is better than that of sensor mentioned above. The proposed electric field intensity sensor has huge prospect in largely remote electric field monitor.

II. Working Principle

The schematic diagram of our device is shown in Fig. 1(a). It is composed of SMF, PCF and SMF successively. PCF is made of pure silica with large mode area. LC is filled with five circles of air holes in the cladding of the fiber, and the holes in the splicing area completely collapse during the welding process. The core mode light from the inlet SMF is coupled to the PCF at the first splicing point. When light passes through the folded fiber segment, both core and cladding modes are generated. These two modes recombine in the second fusion splicing region, thus forming the interference of MZI. The interference spectrum determined by the phase difference between the two modes generated during propagation along PCF can be described as [12]:

$$I = I_1 + I_2 + 2\sqrt{I_1 I_2} COS\left[2\pi L\left(n_{eff}^{cl} - \frac{n_{cm,n}^{eff}}{\lambda}\right)\right] \quad (1)$$

I_1 and I_2 are the output light intensity of core mode and all cladding mode respectively. L represents the coherence length, which is the length of PCF equals to 20mm. n_{eff}^{cl} is the effective refractive index of the core mode, and $n_{cm,n}^{eff}$ is the effective refractive index of the cladding mode. λ is the wavelength of incident light. The phase difference can be expressed as [12]:

$$\Delta\varphi = 2\pi L\left(n_{cl}^{eff} - n_{cm,n}^{eff}\right)/\lambda \quad (2)$$

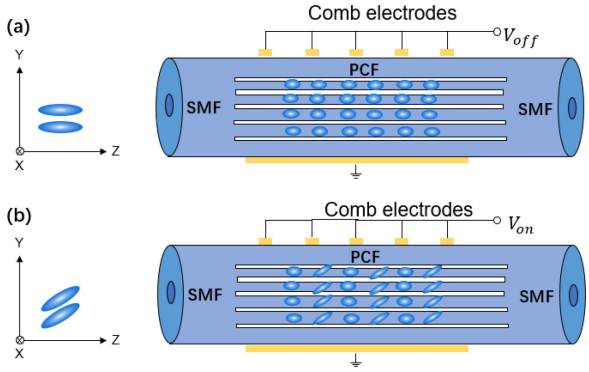

Fig. 2. (a) The LC molecule is parallel to the optical axis when the electric field is off; (b) The switch is turned on and the LC molecule rotates under the electric field.

As $\Delta\varphi = (2m+1)$ (m is an integer), an output dip can be obtained due to interference, and the m_{th} dip wavelength can be represented as [12]:

$$\lambda_{dip} = 2L\left(n_{cl}^{eff} - n_{cm,n}^{eff}\right)/(2m+1) \quad (3)$$

In this paper, the vertical uniform electric field generated by the upper and lower electrodes is used to adjust the alignment of LC molecules along the electric field direction. If the electric light is off, the initial alignment of the liquid crystal is fixed. When the AC power supply is turned on, the orientation of the liquid crystal is controlled by the AC power supply and changes with the electric field. As a result, the refractive index of the material changes and the wavelength shifts. As shown in Fig. 2(a) and (b). The electric field of LC [14] has a Frederick transform threshold. When nematic liquid crystal E7 is filled with PCF fiber, the initial LC molecules are arranged along the axial direction of the pore. When the LC molecule rotates when it is greater than the change threshold. The Frederick transform threshold can be expressed as [13]:

$$\theta = \frac{\pi}{2} - 2tan^{-1}\left[\exp\left(-\frac{E_{eff} - E_{th}}{30E_{th}}\right)\right], E_{eff} > E_{th} \quad (4)$$

Where E_{th} is the threshold electric field that depends on LC properties, E_{eff} is the effective electric field that determines the alignment of LC. When the electric field is higher than E_{th}, LC molecules rearrange along the PCF channel, and the Angle varies with the electric field. RI of LC molecule in two axial directions can be expressed as [17]:

$$n_x = n_0 \quad (5)$$

$$n_y = \left(\frac{sin^2(\theta)}{n_e^2} + \frac{cos^2(\theta)}{n_o^2}\right)^{-\frac{1}{2}} \quad (6)$$

n_0 is the ordinary refractive index of LC. n_e is the special refractive index of LC. The effective RI of LC can be expressed as:

$$n_{eff} = \sqrt{\frac{n_y^2 + n_x^2}{3}} \quad (7)$$

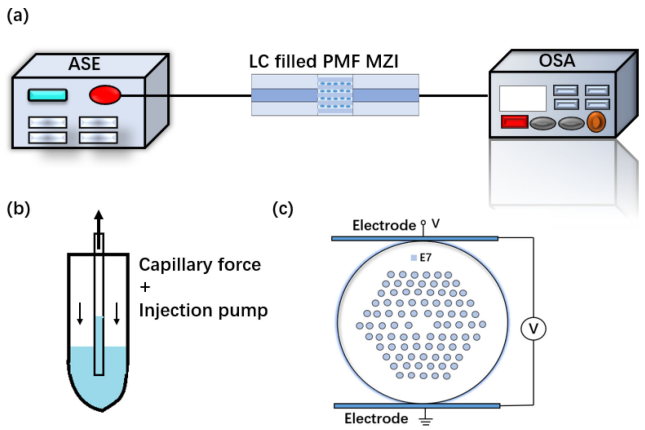

Fig. 3. (a) Schematic diagram of the pre-experimental device; (b) Schematic of the setup for the PCF liquid-crystal filling; and (c) Cross section of the designed PCF.

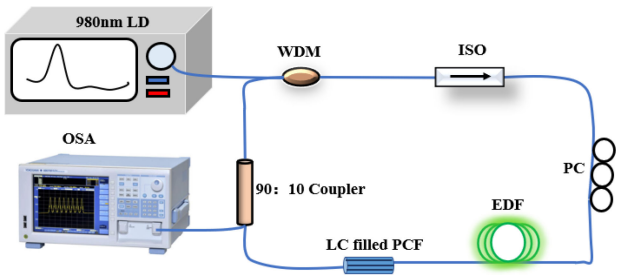

Fig. 4. The intracavity sensing system based on FRL.

III. Experiment Results and Discussion

In order to verify the feasibility of the experiment, a super continuous light source, and an optical spectrum analyzer (OSA, Yokogawa, AQ-6370B) were initially used to measure the transmission spectrum of LC filled PCF, as shown in Fig. 3(a). Besides, as shown in Fig. 3(b), one end of PCF with a length of 20 mm was sealed in a hollow tube connected with the syringe, and the other end was soaked in a bottle containing E7. Liquid crystal is injected into PCF under capillary effect and pressure by pulling syringe. Both ends of PCF are connected with ITO conductive glass, and 2 kHz AC is introduced into ITO, as shown in Fig. 3(c).

Fig. 4 shows the diagram of the experimental device. A 980 nm pumped laser (pl-974-500-fc/apc-p-m) passes through a WDM into the ring cavity as the pump source, with a maximum pumping power of 600 mW. An optical isolator is used to avoid backscattering light from hurting the pump source, and a polarization-maintaining controller is used to control the polarization state in the cavity. In addition, a 1.6 meter erbium-doped fiber is used as gain medium and PCF as sensing unit. The light passes through a 90:10 coupler into the optical spectrum analyzer (Yokogawa AQ6370D) for analysis.

Broadband light source was used to pre-verify the feasibility of the experiment, as shown in Fig. 5. Found at lower electric field than driving liquid crystal. The spectrum is pretty much the same. As the driving voltage is less than the effective voltage regulated by the liquid crystal as shown in equation (4),

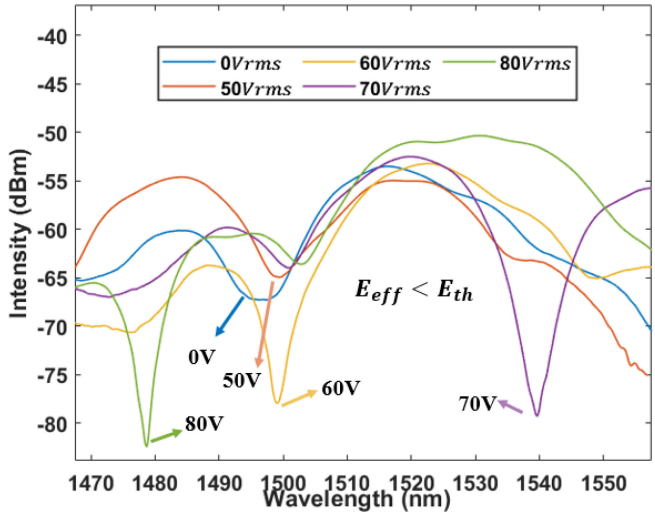

Fig. 5. Transmission spectrum evolution.

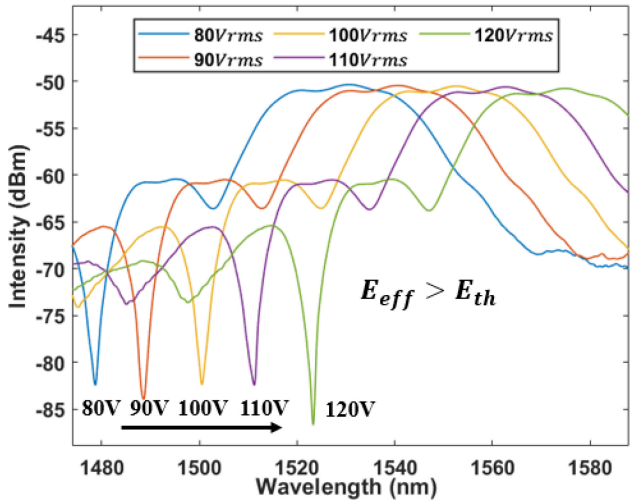

Fig. 6. Resonance wavelengths of the PCF device under 2 kHz AC voltages applied of 80 to 120 Vrms.

the spectrum shown in Fig. 5 presents a chaotic state. When the voltage reaches 80 Vrms, a more obvious peak A appears. When the electric field increases further, as shown in Fig. 6, When the voltage rises from 80V, the spectrum redshifts as the voltage increases. This is because the driving voltage is already greater than the voltage threshold of the modulated liquid crystal. Moving to a longer wavelength. At this time, the liquid crystal is modulated by a 2 2 kHz ac electric field greater than the threshold. Fig. 7 shows that the wavelength shift caused by the modulation electric field has a good linearity. The detection sensitivity is up to 1.11 nm/Vrms, and the linear fitting square is up to 0.998.

In order to verify the good one-to-one correspondence between laser and broadband light source. We will make a corresponding comparison between the ore belt light source and the pumped laser under the driving voltage of 2 kHz AC and the amplitude of 80 V. It is found that the pumped laser appears at the peak-to-peak values of the injected LC PCF-MZI interference.

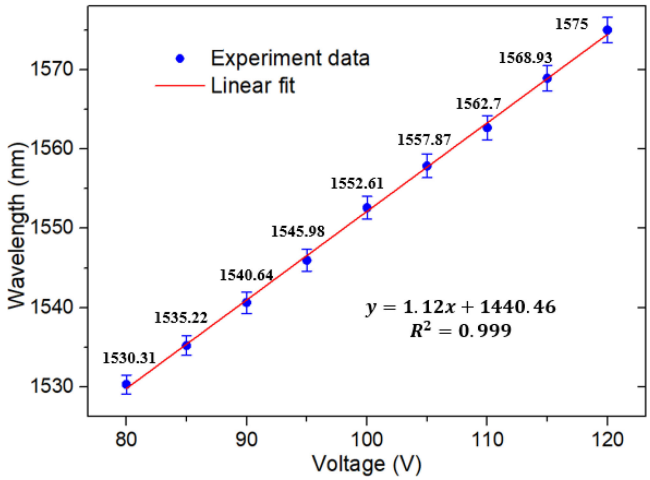

Fig. 7. Linear fitting and error bars of the relationship between voltage and wavelength shift. (From 80 Vrms to 120 Vrms).

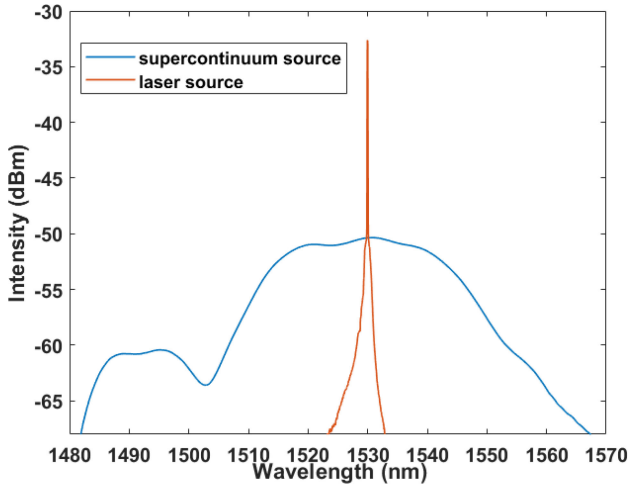

Fig. 8. Output spectrum of the sensor in ASE (blue line) and laser source (orange line).

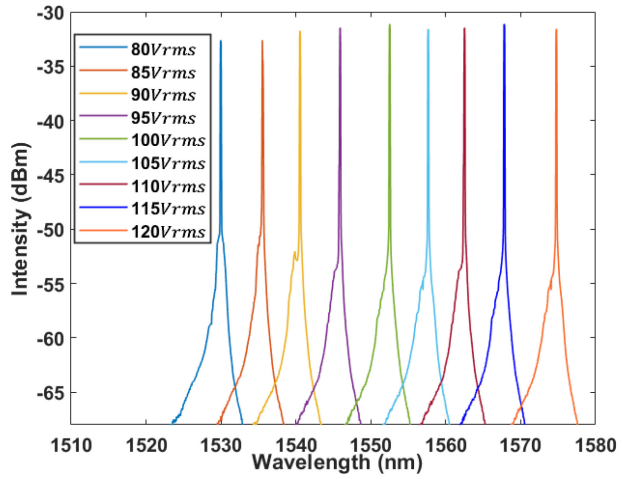

Fig. 9. Output spectrum of the fiber laser electric field intensity sensor system when V changes from 80 Vrms to 120 Vrms with the steps of 5 Vrms.

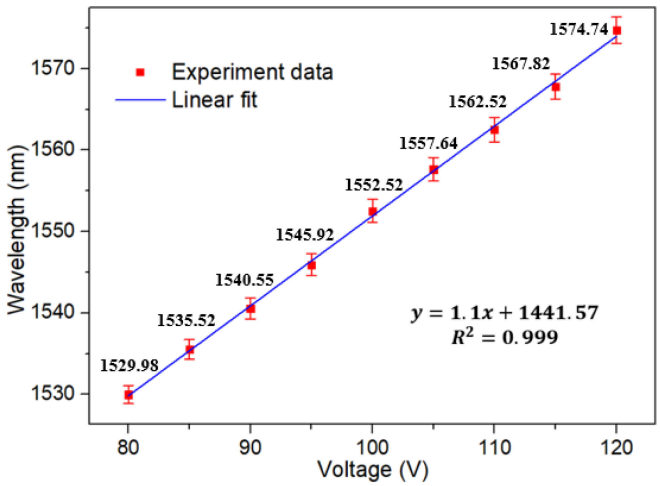

Fig. 10. Linear fitting and error bars of the relationship between RI and wavelength shift.

SNR is better than 35 dB, and 3 dB bandwidth is less than 0.15 nm, as shown in Fig. 8. It is verified that laser can be a good substitute for broadband light source for sensing experiment.

Experimental results are shown in Figs. 9 and 10. As the voltage increases gradually, the wavelength shifts red. From 1530 nm to 1575 nm. It is worth noting that this is almost the limit of gain bandwidth of erbium-doped fiber. Meanwhile, the sensitivity was 1.1nm/Vrms. The results are in good agreement with the test results of broadband light source, which verifies the accuracy of FRL as a sensor. The corresponding linear fitting coefficient is 0.999, indicating that the shift of single peak output wavelength has a good linear fitting with the electric field. It is worth noting that the voltage range selected in this experiment is $80v_{rms}$–$120v_{rms}$. This is because further increasing the voltage value will lead to laser mode hopping, which is limited by the FRL sensor itself rather than the selected material.

The wavelength and power fluctuations of the FRL system are shown in Fig. 11, which are used to quantitatively analyze the stability of the FRL sensor system filled with liquid crystal PCF. In 2.5 hours, the output laser wavelength and intensity remain stable at 80Vrms with only 0.5 dB and 0.15 nm variation, which verifies the possibility of the sensor as a stable sensor.

Using FRL to demodulate optical sensor device information has great improvement not only in the sensitivity and SNR but also in the practical application. The different electric field sensor structures are compared as Table I.

The result shows that FRL has incredible improvement in sensor sensitivity. The sensitivity of LC-filled PCF in Table I is only 0.42 nm/V. The FRL demodulation result has as twice as traditional structures. That's because the wavelength of laser can be easily influenced by external optical parameters vibration. At the same time, when the laser pump condition forms, the tiny destruction which does not change the laser gain and loss region has no influence on central wavelength. That's why the stability of FRL is wonderful.

The LC-PCF used in electric field sensor has various improvement method, such as selective LC material, different interference structures, and custom-build PCF. Even if the highest

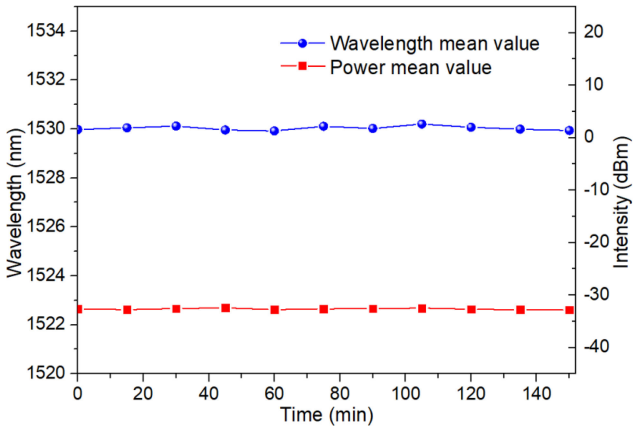

Fig. 11. Test for time stability of wavelength shift and power fluctuation.

TABLE I
SENSITIVITY COMPARISON WITH OTHER ELECTRIC FIELD SENSING STRUCTURES

Sensor structure	Sensitivity	Reference
LC-filled PCF	0.42 nm/Vrms	[10]
LC-PCF in Sagnac ring	0.53 nm/Vrms	[11]
LC-Polarization Maintaining fiber	0.44nm/V(DC)	[18]
LC-Large mode area fiber	0.42nm/Vrms	[19]
LC-filled PM-PCF	1.113 nm/Vrms	[20]
LC-PCF ring laser	1.1 nm/Vrms	Current Work

sensitivity of electric field sensor is as high as 3.49 nm/V [9]. However, it is just partial spectrum results and has little practical application in electric field sensor. FRL sensor uses laser central wavelength shift to demodulate the sensing information and does not need choose a suitably partial spectrum. Therefore, the proposed sensor not only improves the characteristics of the sensor, but also has practical significance in electric field detection

IV. CONCLUSION

A liquid crystal infiltrated PCF-MZI based on liquid crystal filling is proposed for electric field intensity sensing in FRL system. Thanks to the electro-optic effect of the liquid crystal, the sensitivity of the designed sensor is up to 1.1 nm/Vrms. In addition, PCF is used as both sensor and filter, and the SNR of the output laser is up to 35 dB, and the 3-dB bandwidth is less than 0.15 nm. Therefore, the electric field sensor with good photoelectric performance has a good application prospect in photoelectric modulator and high voltage electric field detection.

REFERENCES

[1] T. Pustelny and B. M. Pustelny, "Optical fiber electric field intensity sensor," in *Proc. SPIE 4516, Optoelectron. Electron. Sens. IV*, Aug. 2001, doi: 10.1117/12.435925.
[2] P. Yin *et al.*, "2D materials for nonlinear photonics and electro-optical applications," *Adv. Mater. Interfaces*, vol. 8, no. 14, 2021, Art. no. 2100367.
[3] X. Chen *et al.*, "Liquid crystal-embedded tilted fiber grating electric field intensity sensor," *J. Lightw. Technol.*, vol. 35, no. 16, pp. 3347–3353, Aug. 2017.
[4] Y. Liu, C. Zhao, Y. Zhang, G. Ma, X. Li, and Y. Zhao, "Electrically tunable optical fiber device based on hollow-core fiber infiltrated with liquid crystal," *Sensors Actuators A: Phys.*, vol. 318, 2021, Art. no. 112500.
[5] Y. Huang *et al.*, "Liquid-crystal-filled side-hole fiber for high-sensitivity temperature and electric field measurement," *Micromachines (Basel)*, vol. 10, no. 11, Nov. 2019, Art. no. 761.
[6] N. Q. Ngo, S. Y. Li, R. T. Zheng, S. C. Tjin, and P. Shum, "Electrically tunable dispersion compensator with fixed center wavelength using fiber bragg grating," *J. Lightw. Technol.*, vol. 21, no. 6, pp. 1568–1575, 2003.
[7] T. Alkeskjold *et al.*, "All-optical modulation in dye-doped nematic liquid crystal photonic bandgap fibers," *Opt Exp.*, vol. 12, no. 24, pp. 5857–5871, Nov. 2004.
[8] Q. Liu *et al.*, "Electrically sensing characteristics of the sagnac interferometer embedded with a liquid crystal-infiltrated photonic crystal fiber," *IEEE Trans. Instrum. Meas.*, vol. 70, 2021, Art. no. 9511209.
[9] M. Ma *et al.*, "Highly sensitive temperature sensor based on sagnac interferometer with liquid crystal photonic crystal fibers," *Optik*, vol. 179, pp. 665–671, 2019.
[10] L. Wei *et al.*, "Continuously tunable all-in-fiber devices based on thermal and electrical control of negative dielectric anisotropy liquid crystal photonic bandgap fibers," *Appl. Opt.*, vol. 48, no. 3, pp. 497–503, 2009.
[11] J. Du *et al.*, "Electrically tunable sagnac filter based on a photonic bandgap fiber with liquid crystal infused," *Opt. Lett.*, vol. 33, no. 19, pp. 2215–2217, 2008.
[12] Y. Huang *et al.*, "Tunable electro-optical modulator based on a photonic crystal fiber selectively filled with liquid crystal," *J. Lightw. Technol.*, vol. 37, no. 9, pp. 1903–1908, 2019.
[13] T. Li *et al.*, "Humidity sensor with a PVA-coated photonic crystal fiber interferometer," *IEEE Sensors J.*, vol. 13, no. 6, pp. 2214–2216, Jun. 2013.
[14] J. Lao *et al.*, "In situ plasmonic optical fiber detection of the state of charge of supercapacitors for renewable energy storage," *Light. Sci. Appl.*, vol. 7, 2018, Art. no. 34.
[15] P. Sezemsky *et al.*, "Tailoring properties of indium tin oxide thin films for their work in both electrochemical and optical label-free sensing systems," *Sensors Actuators B: Chem.*, vol. 343, 2021, Art. no. 130173.
[16] J. Huang *et al.*, "Monitoring battery electrolyte chemistry via in-operando tilted fiber Bragg grating sensors," *Energy Environ. Sci.*, vol. 14, no. 12, pp. 64647–6475, 2021.
[17] Y. Liu *et al.*, "Electrically tunable optical fiber device based on hollow-core fiber infiltrated with liquid crystal," *Sensors Actuators A: Phys.*, vol. 318, 2021, Art. no. 112500.
[18] L. Wei, L. Eskildsen, J. Weirich, L. Scolari, T. T. Alkeskjold, and A. Bjarklev, "Continuously tunable all-in-fiber devices based on thermal and electrical control of negative dielectric anisotropy liquid crystal photonic bandgap fibers," *Appl. Opt.*, vol. 48, no. 3, pp. 497–503, Jan. 2009.
[19] S. Mathews *et al.*, "Electronic tunability of ferroelectric liquid crystal infiltrated photonic crystal fibre," *Electron. Lett.*, vol. 45, no. 12, pp. 617–618, 2009.
[20] C. Zhao, L. Cai, and Y. Zhao, "An optical fiber electric field sensor based on polarization-maintaining photonic crystal fiber selectively filled with liquid crystal," *Microelectronic Eng.*, vol. 250, 2021, Art. no. 111639.